RSC Advances

RSC Publishing

PAPER

View Article Online
View Journal | View Issue

Cite this: *RSC Adv.*, 2013, **3**, 20862

Photodegradation of RhB over YVO_4/g-C_3N_4 composites under visible light irradiation†

Jun Cai,[a] Yiming He,*[a] Xiaoxing Wang,[a] Lihong Zhang,[a] Lvzhuo Dong,[b] Hongjun Lin,[c] Leihong Zhao,[b] Xiaodong Yi,[d] Weizheng Weng[d] and Huilin Wan[d]

Received 13th July 2013
Accepted 23rd August 2013

DOI: 10.1039/c3ra43592j

www.rsc.org/advances

A series of novel YVO_4/g-C_3N_4 photocatalysts were prepared by a facile mixing and calcination method. The obtained composites were characterized by X-ray diffraction, Fourier transform infrared spectroscopy, transmission electron microscopy, ultraviolet visible diffuse reflection spectroscopy, X-ray photoelectron spectroscopy, photoluminescence spectroscopy, and a photocurrent–time experiment. The rhodamine B dye was selected as a model pollutant to evaluate the photocatalytic activity of the as-prepared YVO_4/g-C_3N_4 composite. It shows that the photocatalytic activity of g-C_3N_4 can be largely improved by the doping of YVO_4. The optimal YVO_4 content is determined to be 25.8 wt%; and the corresponding degradation rate is 2.34 h^{-1}, about 2.75 folds that of pure g-C_3N_4. A possible mechanism of YVO_4 on the enhancement of visible light performance is proposed. It suggests that YVO_4 plays a key role, which may lead to efficiently suppressing the recombination of photogenerated charge carriers, consequently, improving the visible light photoactivity.

1. Introduction

Semiconductor photocatalysis, which is known as a renewable and sustainable technology, has attracted a great deal of interest due to its universal applications especially in water/air purification, water splitting, and selective organic transformations to fine chemicals.[1–3] The development of high performance photocatalysts, especially the visible-light-driven (VLD) photocatalysts is highly significant for the diverse applications of this clean technology because visible light occupies 43% of the solar spectrum. Two approaches are usually applied to develop VLD photocatalysts. One is preparing a novel visible light responsive material (such as $BiVO_4$, $CaBi_6O_{10}$, $Bi_{12}TiO_{20}$, Ag_3PO_4),[4–8] another way is doping the conventional photocatalyst (such as TiO_2 and ZnO) with transition metals (Fe, Co, W, *etc.*),[9,10] nonmetal elements (N, S, I, F, *etc.*),[11,12] or secondary semiconductors.[13,14]

Recently, a series of orthovanadates (such as $InVO_4$, $BiVO_4$, YVO_4, and $CeVO_4$) has been reported to show good photocatalytic activity for water decomposition and/or the degradation of organic pollutants.[15–20] Most of them exhibit the ability to absorb visible light, which can be mainly attributed to the special electron configuration of the cations (such as Bi^{3+}, Ce^{3+}, Sm^{3+}). Take $BiVO_4$ as the example, it has been reported that its valence band (VB) consists of hybridized Bi6s and O2p orbitals.[16] This hybridization narrows the band gap and makes the semiconductor able to absorb light with a wavelength lower than 553 nm. This explanation can also be used to elucidate the visible-light-responsiveness of lanthanide orthovanadates (such as $GdVO_4$ and $SmVO_4$). The lanthanide cations have a partially filled 4f orbital, which can hybridize with the O2p orbital to decrease the band gap. Different from $GdVO_4$ or $SmVO_4$, YVO_4 has a much wider band gap of 3.38 eV due to the empty 4f orbital of Y.[21] That means YVO_4 can only be irradiated by the light with a wavelength lower than 367 nm. Of course, the large band gap also brings YVO_4 a benefit. The photoexcited electrons and holes in YVO_4 would exhibit a strong redox ability, which induces YVO_4 to exhibit high photocatalytic activity under UV light.[17] Therefore, YVO_4 might serve as a potential and efficient VLD photocatalyst by modification, as shown with TiO_2 and ZnO before. As to our knowledge, however, little research concerned with YVO_4 has been reported.[21] In our opinion, the main reason might be the more negative CB potential of YVO_4 than that of TiO_2. Based on the literature reported,[6] the CB potential of YVO_4 and TiO_2 is estimated to be about −0.21 eV and −0.06 eV, respectively. It should be noted that the real value would be more negative than the estimated value. Few semiconductors contain so negative a CB that could be used to sensitize YVO_4.

[a]*Department of Materials Physics, Zhejiang Normal University, Jinhua, 321004, China. E-mail: hym@zjnu.cn; Fax: +86-0579-83714946; Tel: +86-0579-83792294*

[b]*Institute of Physical Chemistry, Zhejiang Key Laboratory for Reactive Chemistry on Solid Surfaces, Zhejiang Normal University, Jinhua, 321004, China*

[c]*College of Geography and Environmental Sciences, Zhejiang Normal University, Jinhua, 321004, China*

[d]*State Key Laboratory Physical Chemistry of Solid Surfaces, Xiamen University, Xiamen 361005, PR China*

† Electronic supplementary information (ESI) available: TG-DTA profiles of g-C_3N_4 and YVO_4/g-C_3N_4 composite (Fig. S1); XPS spectra C1s, N1s, V3d, and Y3d (Fig. S2); X-ray elemental maps of 25.8% YVO_4/g-C_3N_4 composite (Fig. S3); XRD patterns of 25.8% YVO_4/g-C_3N_4 composite before and after reaction (Fig. S4). See DOI: 10.1039/c3ra43592j

Polymeric graphite-like carbon nitride (g-C_3N_4) is a metal-free semiconductor which can be synthesized by the simple heating of urea/melamine at 500–600 °C.[22,23] It is very cheap and considered as a "sustainable" material. Different from the other polymer materials, g-C_3N_4 presents high thermal and chemical stability. It is found be stable in air flow below 500 °C and in solution with pH = 0–14. Besides, g-C_3N_4 can absorb visible light due to its moderate band gap (2.7 eV). These superior properties indicate that the metal-free g-C_3N_4 has numerous potential applications in the field of photocatalysis. Since Wang and Yan *et al.* first demonstrated the great prospect of g-C_3N_4 in dye degradation and water splitting in 2009,[23,24] a large quantity of studies have been reported. In our opinion, however, there was still another advantage which was not listed above which makes g-C_3N_4 so interesting. The valence band XPS experiment shows that the CB potential of g-C_3N_4 is located at approximately −1.50 eV.[25] Nearly all of the semiconductors can be coupled with g-C_3N_4 to form a new composite photocatalyst. That's why so many types of g-C_3N_4 based photocatalysts have been reported.[25–30] Besides, this special property indicates that g-C_3N_4 might be a suitable semiconductor to modify the YVO_4 photocatalyst.

In this paper, a kind of novel g-C_3N_4/YVO_4 composite photocatalysts were prepared for the first time *via* mixing and heating methods. Rhodamine B (RhB) was used as a model compound to investigate the activities of YVO_4/g-C_3N_4 composite under visible light illumination (λ > 420 nm). The investigation result indicates the YVO_4/g-C_3N_4 composite catalysts show strong photocatalytic activity as well as high photocatalytic stability. On the basis of the investigation results, the origin of the high photocatalytic activity is discussed.

2. Experimental

2.1 Preparation of catalysts

All chemicals were reagent grade and used without further purification. N-doped TiO_2 was prepared by a modified sol–gel method.[26] Pure g-C_3N_4 powders were prepared by directly calcining melamine at 520 °C for 4 h. Pure YVO_4 was prepared by a hydrothermal method: solutions of NH_4VO_3 and $Y(NO_3)_3$ (obtained by dissolving Y_2O_3 in HNO_3 solution) with a V to Y mole ratio of 1 : 1 were mixed to give a deposit. The pH value of the solution was adjusted to 7 by a solution of NH_3. The mixture was transferred into a 100 mL autoclave with an inner Teflon lining and maintained at 180 °C for 12 h. The resulting white precipitate was collected by filtration and washed several times with deionized water before drying the sample in an oven at 80 °C for 12 h.

The YVO_4/g-C_3N_4 composites containing 5.9%, 13.2%, 25.8%, 32.1%, and 42.9% YVO_4 were prepared by a mixing-calcination method. YVO_4 and g-C_3N_4 with different weight ratios were mixed and ground in an agate mortar for 20 min. Then, the mixture was calcined at 450 °C for 2 h to obtain the YVO_4/g-C_3N_4 catalyst. The weight concentration of YVO_4 was determined by TG-DTA experiment (see Fig. S1†). For comparison, pure YVO_4 was also heated at 450 °C for 2 h.

2.2 Photocatalytic experiments

The photocatalytic degradation of 10 ppm RhB under visible-light irradiation was used to evaluate the activities of the synthesized powders. The light source for photocatalysis was a spherical Xe lamp (350 W). Two optical filters were used to eliminate the UV light and infrared light (800 nm > λ > 420 nm). The power density at the position of the reactor is about 7.4 mW cm^{-2}. The volume of initial RhB solution is 300 mL. All powder contents in the RhB aqueous solution are 0.10 g per 100 mL. Prior to irradiation, the mixture was agitated for an hour to ensure adsorption–desorption equilibrium at room temperature. At regular intervals, samples were withdrawn and centrifuged to separate solid particles for analysis. The concentration of aqueous RhB was determined using a UV-vis spectrophotometer at 554 nm by measuring its absorbance. The RhB degradation was calculated by the Lambert–Beer equation. Photoactivities for RhB in the absence of the photocatalyst were also evaluated.

2.3 Characterizations

Thermogravimetry analysis (TG-DTA; Netzsch STA449) was carried out in a flow of air (10 mL min^{-1}) at a heating rate of 10 °C min^{-1}. The XRD characterization of catalysts was carried out on Philips PW3040/60 using Cu Kα radiation (40 kV per 40 mA). The Fourier transform infrared spectroscopy (FT-IR) spectra of the catalysts were recorded on Nicolet NEXUS670 with a resolution of 4 cm^{-1}. The X-ray photoelectron spectroscopy (XPS) measurements were performed with a Quantum 2000 Scanning ESCA Microprobe instrument using Al Kα. The C1s signal was set to a position of 284.6 eV. The specific surface areas were measured on an Autosorb-1 (Quantachrome Instruments) by the Brunauer–Emmett–Teller (BET) method. The SEM pictures were taken on a field emission scanning electron microscope (LEO-1530). The HRTEM images were collected with a JEM-2010F transmission electron microscope at an accelerating voltage of 200 kV. The UV-vis diffuse reflectance spectra (DRS) of catalysts were recorded on a UV-vis spectrometer (PerkinElmer Lambda900) equipped with an integrating sphere. The photoluminescence (PL) spectra were collected on an FLS-920 spectrometer (Edinbergh Instrument), using a Xe lamp (excitation at 312 nm) as a light source.

The photocurrent–time experiment (PT) was measured with an electrochemical analyzer (CHI660B) in a two-electrode system under zero bias. The prepared sample and a Pt wire work as the working electrode and the counter electrode, respectively. The light source is a 500 W Xe arc lamp equipped with a UV-cutoff filter (λ > 420 nm). Na_2SO_4 (0.5 mol L^{-1}) aqueous solution was used as the electrolyte. The preparation of the working electrode refers to the previous literature.[26]

3. Results and discussion

3.1 Characterization of catalysts

The structure of the synthesized YVO_4/g-C_3N_4 hybrids was characterized by XRD and FT-IR. Fig. 1 shows the XRD patterns of the composites. Pure g-C_3N_4 shows a strong diffraction peak at 27.4 °C, which can be indexed to the (002) diffraction planes

of the graphite-like carbon nitride and correspond to the characteristic interplanar stacking peaks of aromatic systems.[23] Pure YVO_4 is in its tetragonal phase and exhibits the strong characteristic peaks at 19.0°, 25.2°, 33.8°, 50.0°, and 51.6° (JCPDS 17-0341). For YVO_4/g-C_3N_4 composites, the XRD patterns proved that no impurity existed. Only YVO_4 and g-C_3N_4 phases were observed. With an increasing amount of YVO_4 from 5.9% to 42.9%, the diffraction peaks of YVO_4 are intensified gradually, whereas the peaks of g-C_3N_4 are weakened. The relationship between the g-C_3N_4 content and its corresponding peak intensity is not so obvious in the FT-IR spectra. As shown in Fig. 2, the FT-IR spectra of YVO_4/g-C_3N_4 composites are similar to that of pure g-C_3N_4. All the YVO_4/g-C_3N_4 composites exhibit several strong IR peaks at 1250 cm^{-1}, 1325 cm^{-1}, 1414 cm^{-1}, 1569 cm^{-1}, 1636 cm^{-1} which are related to the aromatic C–N stretching mode and C=N stretching vibration modes of g-C_3N_4.[31] However, at the region of 814–840 cm^{-1}, the influence of YVO_4 content can still be observed. YVO_4 has a strong characteristic peak at 829 cm^{-1} which can be attributed to the V–O stretching vibration mode,[21] while g-C_3N_4 exhibits a sharp peak at 809 cm^{-1} originated from an *s*-triazine ring system.[23] With the increase of YVO_4 concentration in YVO_4/g-C_3N_4 composites, the IR peak at 809 cm^{-1} is strengthened and shifts to higher wavenumber, which is consistent with the result of XRD.

The XPS was obtained to analyze the oxidation state and the surface chemical composition of the YVO_4/g-C_3N_4 composite. Fig. 3 provides the XPS spectra of g-C_3N_4, YVO_4 and a representative photocatalyst 25.8% YVO_4/g-C_3N_4 composite. As shown in Fig. 3a, g-C_3N_4 presents a simple spectrum containing the signals of C1s, N1s, and O1s, while YVO_4 exhibits a more complicated XPS spectrum due to the contribution of V and Y. For the 25.8% YVO_4/g-C_3N_4 composite, its spectrum can be seen as the combination of that of g-C_3N_4 and YVO_4. The binding energies of C1s, N1s, Y3$d_{5/2}$, V2$p_{3/2}$ were determined to be 287.9 eV, 397.7 eV, 156.8 eV (Y^{3+}),[32] and 517.1 eV (V^{5+}),[33] respectively (see Fig. S2†). These values are consistent with that of pure phases, indicating that the consisting phases are not changed during the preparation of the composite. This result is in good agreement with the XRD and FT-IR experiments.

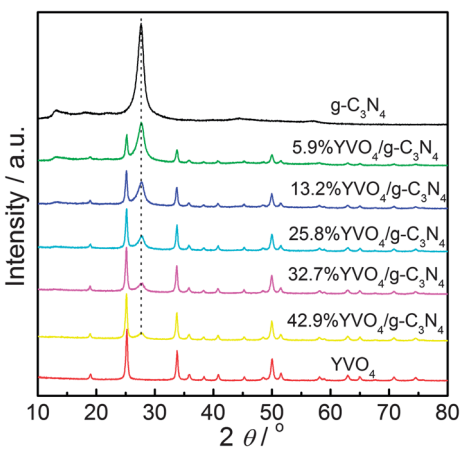

Fig. 1 XRD patterns of YVO_4/g-C_3N_4 composites.

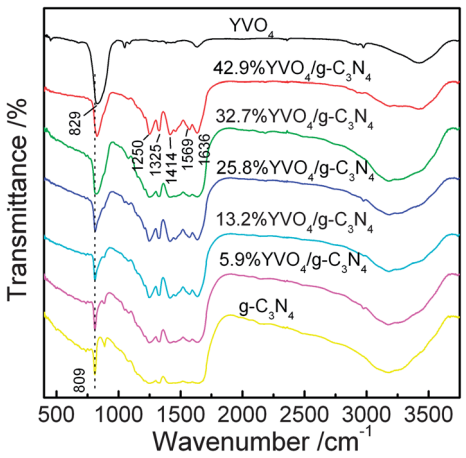

Fig. 2 FT-IR spectra of YVO_4/g-C_3N_4 composites with varied YVO_4 weight content.

The valence band X-ray photoelectron spectroscopy (VB XPS) spectra of YVO_4 and g-C_3N_4 are also shown in Fig. 3b. The position of the valence band edge of g-C_3N_4 locates at about 1.53 eV, which is consistent with the previous result.[25] For YVO_4, the value is about 2.65 eV.

The morphology of the as-prepared samples is revealed by SEM and TEM. Fig. 4a and b show the SEM images of YVO_4 and g-C_3N_4. Pure g-C_3N_4 has a layered structure with many stacking layers (Fig. 4b), whereas the obtained YVO_4 particle has a spherical shape with a diameter of <50 nm (Fig. 4a). The different morphology makes them exhibit different specific surface areas. The BET surface area of g-C_3N_4 is equal to 13 $m^2\ g^{-1}$ which is much smaller than that of YVO_4 (148 $m^2\ g^{-1}$). Fig. 4c shows the SEM image of a representative composite 25.8% YVO_4/g-C_3N_4. The YVO_4 nanoparticles are found deposited on the surface of g-C_3N_4 sheets and randomly distributed. The same result can also be obtained from its TEM picture (Fig. 4d). Besides, considering that the 25.8% YVO_4/g-C_3N_4 hybrid was ultrasonicated during the sample preparation procedure for TEM analysis, the result in Fig. 4d indicates that the interaction between the YVO_4 nanoparticles and g-C_3N_4 layers is very strong, which benefits the formation of a heterojunction of YVO_4 and g-C_3N_4. An X-ray elemental map of the sample was also carried out to investigate the dispersion of consisting phases. The result shown in Fig. S3† suggests that both g-C_3N_4 and YVO_4 are dispersed homogeneously in the composite. The fine dispersal of YVO_4 can increase the interface amounts of g-C_3N_4 and YVO_4, which might promote the separation of electron–hole pairs and, subsequently accelerate photocatalytic reaction. The specific surface area of the 25.8% YVO_4/g-C_3N_4 composite was also determined by the BET method. The value is 30 $m^2\ g^{-1}$. The enlarged surface area in comparison to that of g-C_3N_4 (13 $m^2\ g^{-1}$) can be ascribed to the contribution of YVO_4 (148 $m^2\ g^{-1}$). For the other composite samples, the BET surface areas are 19 $m^2\ g^{-1}$ (5.9% YVO_4/g-C_3N_4), 29 $m^2\ g^{-1}$ (13.2% YVO_4/g-C_3N_4), 35 $m^2\ g^{-1}$ (32.7% YVO_4/g-C_3N_4), 49 $m^2\ g^{-1}$ (42.9% YVO_4/g-C_3N_4), respectively. The values increased as the YVO_4 content increased. However, the

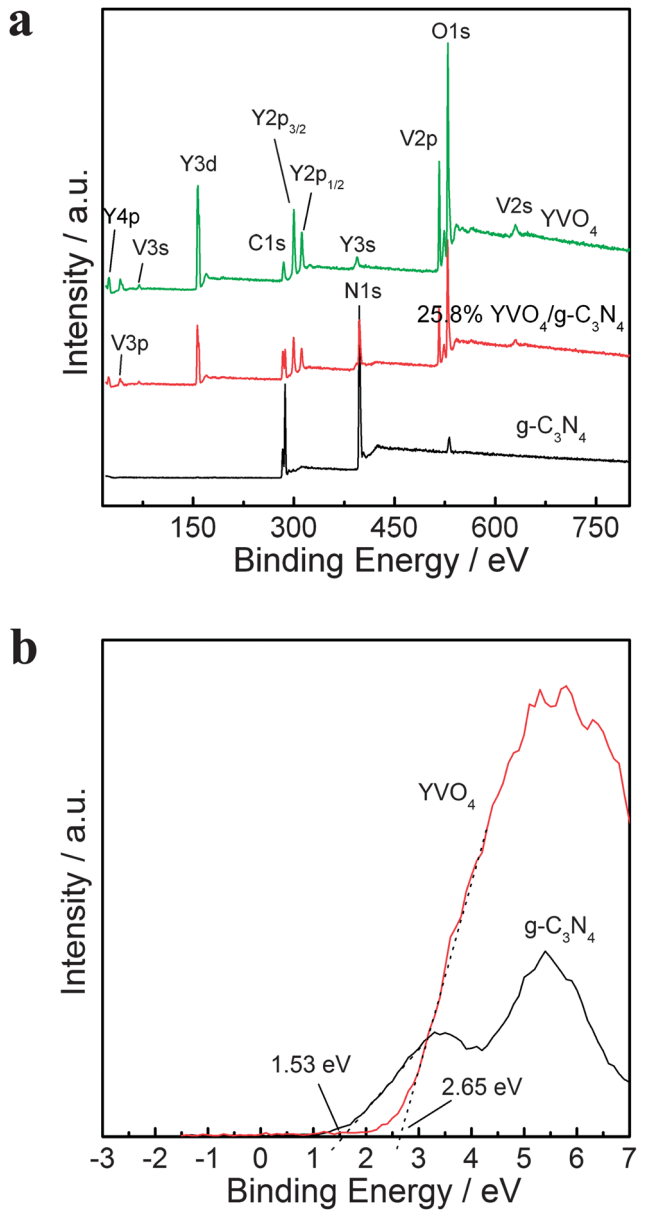

Fig. 3 XPS spectra of g-C_3N_4, YVO_4 and YVO_4/g-C_3N_4 composites (a), and the VB XPS spectra of g-C_3N_4 and YVO_4 (b).

BET surface area of the YVO_4/g-C_3N_4 hybrid is still much smaller than that of YVO_4.

Fig. 5 shows the UV-vis spectra of YVO_4, g-C_3N_4 and YVO_4/g-C_3N_4 hybrids with different YVO_4 concentrations. As can be seen, YVO_4 can only absorb the UV light, whereas g-C_3N_4 displays clear optical response in the visible region. Based on the equation of Kubelka–Munk,[34] the band gaps of YVO_4 and g-C_3N_4 can be determined to be 3.50 eV and 2.70 eV, respectively, which are in good agreement with the reported values.[17,23] The UV-vis spectra of YVO_4/g-C_3N_4 hybrids can be seen as the overlap of that of YVO_4 and g-C_3N_4. As the YVO_4 content increases, the characteristic absorption peak of g-C_3N_4 at about 380 nm is weakened gradually. Each YVO_4/g-C_3N_4 sample exhibits good absorption ability for visible light. But none of them has higher photoabsorption performance than pure g-C_3N_4.

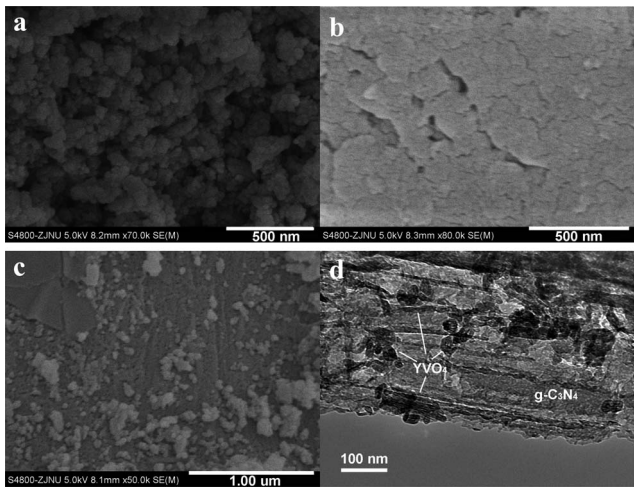

Fig. 4 SEM images of YVO_4 (a), g-C_3N_4 (b) and 25.8% YVO_4/g-C_3N_4 composite (c) and (d) TEM image of 25.8% YVO_4/g-C_3N_4 sample.

3.2 Photocatalytic activity of catalysts

The photocatalytic performance of YVO_4/g-C_3N_4 hybrids was evaluated by the photodegradation of RhB aqueous solution at room temperature under visible light irradiation. The blank test was also carried out under the same condition to investigate the photostability and chemical stability of RhB. No RhB was degraded without the help of the photocatalyst, indicating that RhB is a suitable model dye with high stability under visible light irradiation. Fig. 6 shows the decrease of RhB concentration as a function of time over different photocatalysts. The adsorption process in the dark is also included. As can be seen in Fig. 6a, YVO_4 which has a higher specific surface area presents a poorer adsorption ability for RhB than g-C_3N_4. The same phenomenon is also observed in N–TiO_2 and YVO_4/g-C_3N_4. They have different BET surface areas (the BET value of N–TiO_2 is 68 $m^2\ g^{-1}$), but they exhibit similar adsorption of RhB after one hour adsorption process in the dark. It indicates that there is no close relationship between the surface area and dye adsorption ability for different photocatalysts, which might be due to that the adsorption ability of a catalyst is not only affected by its surface area. Other factors (such as the surface electric charge of a catalyst) can also affect the adsorption of dye.

When the visible light irradiation is on, a small decrease of RhB concentration was observed in the presence of YVO_4. Since

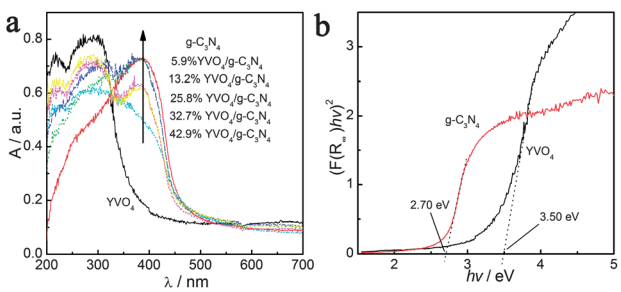

Fig. 5 UV-vis spectra of YVO_4/g-C_3N_4 hybrids with varied YVO_4 weight content (a) and estimated band gap of YVO_4 and g-C_3N_4 by the Kubelka–Munk function (b).

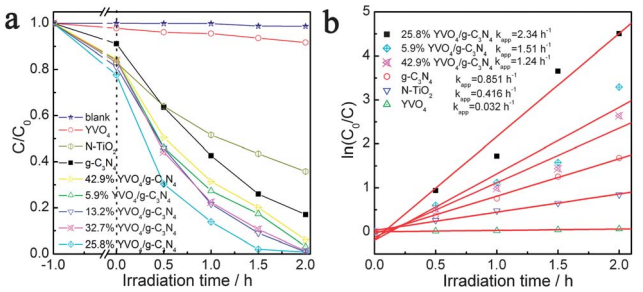

Fig. 6 The decrease of RhB concentration as a function of time over different photocatalysts (a), and their corresponding kinetic constants (b).

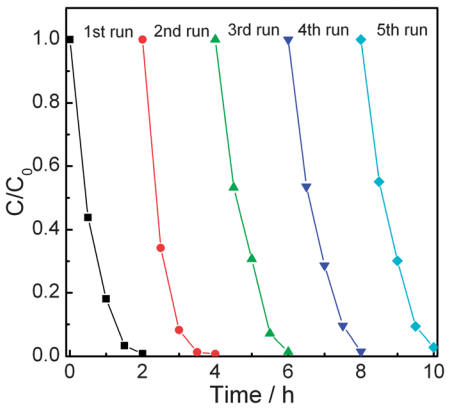

Fig. 7 Cycling runs of 25.8% YVO_4/g-C_3N_4 in the photodegradation of RhB.

YVO_4 cannot absorb visible light, the weak photocatalytic activity might result from the few UV light which passed through the cutoff filter. Different from YVO_4, N–TiO_2 which is usually used as a benchmark of VLD photocatalysts, presents high photoactivity. After visible light irradiation for 120 min, 50% of RhB was bleached. In the case of g-C_3N_4, better photocatalytic efficiency was observed, indicated by reaction time shortening from two hours to one hour for the half degradation of RhB. The coupling of YVO_4 with g-C_3N_4 enhances the photocatalytic efficiency. As can be seen in Fig. 6a, the decrease of RhB concentration became faster in the presence of YVO_4/g-C_3N_4. The optimal content of YVO_4 in YVO_4/g-C_3N_4 hybrids was found to be 25.8 wt% by comparing their photocatalytic efficiency in the degradation of RhB solution.

The kinetic constants corresponding to different photocatalysts were also calculated to evaluate the superiority of YVO_4/g-C_3N_4. The degradation of RhB was found to be a pseudo-first order kinetic process, which can be expressed by the following equation:[30] $\ln(C_0/C) = kt$, where C_0 and C are the initial and measured concentrations of RhB, t and k are degradation time and kinetic constants, respectively. The result shown in Fig. 6b indicates that the 25.8% YVO_4/g-C_3N_4 hybrid has the highest kinetic constant 2.34 h^{-1}, which is 2.75 times and 75 times of that obtained from g-C_3N_4 and N–TiO_2, respectively.

In addition to the photocatalytic efficiency, the catalyst's lifetime is another important parameter of the photocatalytic process, so it is essential to evaluate the stability of the catalyst for practical application. Therefore, the repetition tests for the photodegradation of RhB using 25.8% YVO_4/g-C_3N_4 were performed. The result shown in Fig. 7 revealed that the high photocatalytic activity of YVO_4/g-C_3N_4 for RhB degradation was effectively maintained after five cycle experiments. Only a slight decrease was observed, which can be attributed to the loss of catalyst during the recycle process. Furthermore, the XRD patterns of the photocatalyst before and after reaction indicate that no evident difference was observed (see Fig. S4†). Obviously, the prepared YVO_4/g-C_3N_4 photocatalyst showed good stability during the photocatalytic reaction.

3.3 Discussion

Since the heterogeneous photocatalytic reaction is a surface reaction, the adsorption of reactant is considered as an important factor in affecting the photocatalytic activity. This makes people pay much attention to the catalyst's surface area which is usually correlated with its adsorption ability. In the case of YVO_4/g-C_3N_4, however, two facts indicate that the surface area is not a key factor. First, the data in Fig. 6a displays that the adsorption of RhB is not in agreement with the catalyst's surface area. Second, the YVO_4/g-C_3N_4 composites exhibit similar adsorption abilities for RhB. Therefore, the crucial factor might be the phase composition which induces the efficient separation of electron–hole pairs and the subsequent good photoactivity, just like the other composite photocatalysts.[13,14,21,25]

The XRD and FT-IR characterizations have proven that the YVO_4/g-C_3N_4 photocatalyst is a two-phase composite. The VB XPS experiment shows that the valence band potential of g-C_3N_4 and YVO_4 is about 1.53 eV and 2.65 eV, respectively. Based on the equation of $E_{CB} = E_{VB} - E_g$, the CB edge potentials of g-C_3N_4 can be determined to be −1.17 eV. For YVO_4, the value is −0.85 eV. Clearly, YVO_4 and g-C_3N_4 hold suitable band potentials which triggers them to form the hetero-structures during the heating process. Under visible light irradiation, the photo-induced electrons on the g-C_3N_4 particle surface can easily transfer to YVO_4 *via* the interfaces, while the holes remain on the g-C_3N_4 surface. The electron transfer effectively retards the recombination of electron–hole pairs in the composite and,

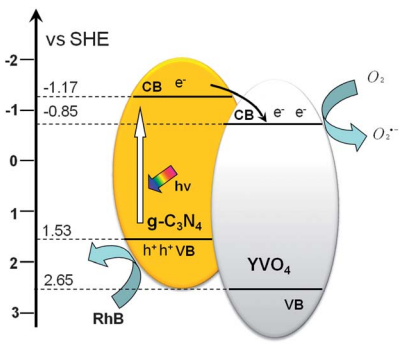

Fig. 8 Scheme for electron–hole transport at the interface of the YVO_4/g-C_3N_4 composite.

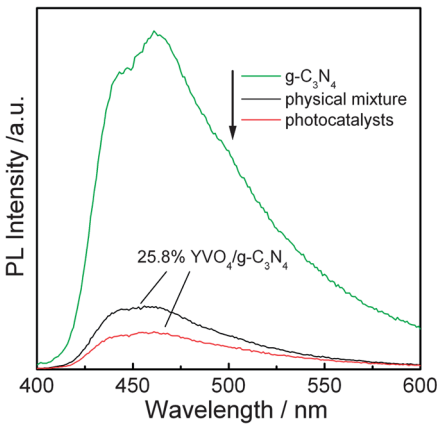

Fig. 9 Photoluminescence spectra of pure g-C_3N_4 and the 25.8% YVO_4/g-C_3N_4 composite.

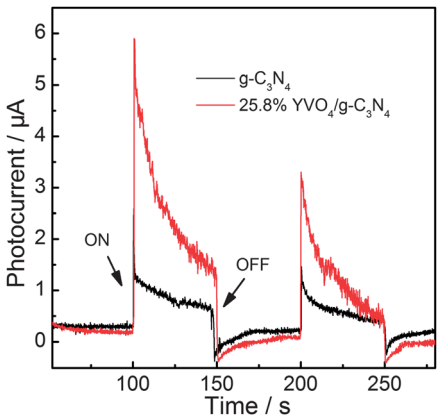

Fig. 10 Transient photocurrent response for g-C_3N_4 and 25.8% YVO_4/g-C_3N_4 samples.

thereby improves the photo-oxidation efficiency. That's why the doping of YVO_4 enhanced the photocatalytic activity of g-C_3N_4. Meanwhile, based on the scheme shown in Fig. 8, it can be deduced that the YVO_4 content was pivotal for achieving the high photocatalytic activity of the YVO_4/g-C_3N_4 composite. The suitable YVO_4 content causes its good dispersion in the catalyst, which benefits the formation of heterojunctions between the g-C_3N_4 and YVO_4 particles. As a result, a high separation of the charge carriers and photocatalytic activity were obtained on the 25.8% YVO_4/g-C_3N_4 sample.

The PL measurement was used to elucidate the separation efficiency of electron–hole pairs in the YVO_4/g-C_3N_4 composite. In general, the recombination of electron–hole pairs would result in PL signals. The stronger the PL peak is, the lower separation efficiency of the catalyst is.[29,35] Fig. 9 shows the PL spectra of g-C_3N_4 and 25.8% YVO_4/g-C_3N_4 photocatalyst. As shown in this figure, g-C_3N_4 shows a strong PL emission at about 460 nm, indicating that the electrons and holes recombine rapidly.[35] However, over the YVO_4/g-C_3N_4 sample, the peak intensity is greatly decreased. This indicates that the doping of YVO_4 suppresses the electron–hole pair recombination. Additionally, it should be noted that the decreased g-C_3N_4 content might also lead to the weakened PL signal. Therefore, in order to rule out the contribution of the decreased g-C_3N_4 content, a physical mixture of YVO_4 and g-C_3N_4 with the same g-C_3N_4 content as the 25.8% YVO_4/g-C_3N_4 sample was also prepared and characterized by PL measurement. The result shown in Fig. 9 indicates that the physical mixture presents a stronger PL peak than the 25.8% YVO_4/g-C_3N_4 composite. It definitely verified that charge transfer exists between YVO_4 and g-C_3N_4, which is in good agreement with the mechanism suggested above.

Besides the PL measurement, the PT technique is also useful to reveal the interfacial charge transfer dynamics between the interfacial surface of YVO_4 and g-C_3N_4 semiconductors. Generally, a high value of the photocurrent indicates that the sample holds strong ability in generating and transferring the photoexcited charge carrier under irradiation.[36,37] Therefore, the g-C_3N_4 and YVO_4/g-C_3N_4 composite are characterized by PT, and the result is shown in Fig. 10. The 25.8% YVO_4/g-C_3N_4 had a higher photocurrent than g-C_3N_4 under the same condition, suggesting that the YVO_4/g-C_3N_4 composite exhibits stronger ability in the separation of electron–hole pairs than g-C_3N_4, as proven by the PL analysis.

4. Conclusion

In summary, a novel YVO_4/g-C_3N_4 composite photocatalyst was successfully synthesized by a simple milling and heating method. The photocatalytic testing result shows that the synthesized composite has a good performance in the photodegradation of RhB. The 25.8% YVO_4/g-C_3N_4 sample exhibits the photodegradation efficiency 2.75 times higher than pure g-C_3N_4. Based on the energy band positions, PL spectra, and photocurrent curves, the enhanced photocatalytic activity was mainly ascribed to the synergy effect between YVO_4 and g-C_3N_4.

Acknowledgements

This work was financially supported by the National Natural Science Foundation of China (21003109, 51108424), the Opening-foundation of State Key Laboratory Physical Chemistry and Solid Surfaces, Xiamen University, China (201311), and the Science Foundation of Zhejiang Normal University (KJ20120028).

Notes and references

1 B. Ohtani, *J. Photochem. Photobiol., C*, 2010, **11**, 157–178.
2 X. B. Chen, S. H. Shen, L. J. Guo and S. S. Mao, *Chem. Rev.*, 2010, **110**, 6503–6570.
3 M. A. Lazar and W. A. Daoud, *RSC Adv.*, 2013, **3**, 4130–4140.
4 S. W. Liu, K. Yin, W. S. Ren, B. Cheng and J. G. Yu, *J. Mater. Chem.*, 2012, **22**, 17759–17767.
5 Y. J. Wang, Y. M. He, T. T. Li, J. Cai, M. F. Luo and L. H. Zhao, *Catal. Commun.*, 2012, **18**, 161–164.
6 T. T. Li, Y. J. Wang, Y. M. He, J. Cai, M. F. Luo and L. H. Zhao, *Mater. Lett.*, 2012, **74**, 170–172.

7 W. Guo, S. Q. Zhang, Y. N. Guo, L. Ma, F. Su, Y. H. Guo and A. F. Geng, *RSC Adv.*, 2013, **3**, 4008–4017.
8 Y. P. Bi, S. X. Ouyang, N. Umezawa, J. Y. Cao and J. H. Ye, *J. Am. Chem. Soc.*, 2011, **133**, 6490–6492.
9 W. Choi, A. Termin and M. R. Hoffmann, *J. Phys. Chem.*, 1994, **98**, 13669–13679.
10 H. Yamashita, M. Harada, J. Misaka, M. Takeuchi, K. Ikeue and M. Anpo, *J. Photochem. Photobiol., A*, 2002, **148**, 257–261.
11 R. Ashi, T. Morikawa, T. Ohwaki, K. Aoki and Y. Taga, *Science*, 2001, **293**, 269–271.
12 S. Sakthivel and H. Kisch, *Angew. Chem., Int. Ed.*, 2003, **42**, 4908–4911.
13 K. K. Akurati, A. Vital, J.-P. Dellemann, K. Michalow, T. Graule, D. Ferri and A. Baiker, *Appl. Catal., B*, 2008, **79**, 53–62.
14 A. Kar, S. Kundu and A. Patra, *RSC Adv.*, 2012, **2**, 10222–10230.
15 S. W. Cao, J. Fang, M. M. Shahjamali, F. Y. C. Boey, J. Barber, S. C. J. Loo and C. Xue, *RSC Adv.*, 2012, **2**, 5513–5515.
16 M. R. Dolgos, A. M. Paraskos, M. W. Stoltzfus, S. C. Yarnell and P. M. Woodward, *J. Solid State Chem.*, 2009, **182**, 1964–1971.
17 H. Y. Xu, H. Wang and H. Yan, *J. Hazard. Mater.*, 2007, **144**, 82–85.
18 S. Mahapatra, G. Madras and T. N. Guru Row, *Ind. Eng. Chem. Res.*, 2007, **46**, 1013–1017.
19 P. A. Deshpande and G. Madras, *Chem. Eng. J.*, 2010, **158**, 571–577.
20 Y. M. He, Y. Wu, T. L. Sheng and X. T. Wu, *J. Hazard. Mater.*, 2010, **180**, 675–682.
21 Y. M. He, Y. Wu, H. Guo, T. L. Sheng and X. T. Wu, *J. Hazard. Mater.*, 2009, **169**, 855–860.
22 J. H. Liu, T. K. Zhang, Z. C. Wang, G. Dawson and W. Chen, *J. Mater. Chem.*, 2011, **21**, 14398–14401.
23 S. C. Yan, Z. S. Li and Z. G. Zou, *Langmuir*, 2009, **25**, 10397–10401.
24 X. C. Wang, K. Maeda, A. Thomas, K. Takanabe, G. Xin, J. M. Carlsson, K. Domen and M. Antonietti, *Nat. Mater.*, 2009, **8**, 76–80.
25 S. C. Yan, S. B. Lv, Z. S. Li and Z. G. Zou, *Dalton Trans.*, 2010, **39**, 1488–1491.
26 T. T. Li, L. H. Zhao, Y. M. He, J. Cai, M. F. Luo and J. J. Lin, *Appl. Catal., B*, 2013, **129**, 255–263.
27 S. Y. Yang, W. Y. Zhou, C. Y. Ge, X. T. Liu, Y. P. Fang and Z. S. Li, *RSC Adv.*, 2013, **3**, 5631–5638.
28 L. Ge, C. C. Han and J. Liu, *Appl. Catal., B*, 2011, **108**, 100–107.
29 Y. M. He, J. Cai, T. T. Li, Y. Wu, Y. M. Yi, L. H. Zhao and M. F. Luo, *Ind. Eng. Chem. Res.*, 2012, **51**, 14729–14737.
30 G. Z. Liao, S. Chen, X. Quan, H. T. Yu and H. M. Zhao, *J. Mater. Chem.*, 2012, **22**, 2721–2726.
31 X. F. Li, J. Zhang, L. H. Shen, Y. M. Ma, W. W. Lei, Q. L. Cui and G. T. Zou, *Appl. Phys. A: Mater. Sci. Process.*, 2009, **94**, 387–392.
32 J. Zhao, B. H. Yao, Q. He and T. Zhang, *J. Hazard. Mater.*, 2012, **229–230**, 151–158.
33 M. Kruczek, E. Talik, H. Sakowska, W. Szyrski, Z. Ujma and D. Skrzypek, *J. Cryst. Growth*, 2005, **275**, e1715–e1720.
34 W. J. Luo, J. W. Tang, Z. G. Zou and J. H. Ye, *J. Alloys Compd.*, 2008, **455**, 346–352.
35 X. Z. Li, F. B. Li, C. L. Yang and W. K. Ge, *J. Photochem. Photobiol., A*, 2001, **141**, 209–217.
36 M. Kong, Y. Z. Li, X. Chen, T. T. Tian, P. F. Fang, F. Zheng and X. J. Zhao, *J. Am. Chem. Soc.*, 2011, **133**, 16414–16417.
37 Q. J. Xiang, J. G. Yu and M. Jaroniec, *J. Phys. Chem. C*, 2011, **115**, 7355–7363.

